

**New Mechanistic Insights to the O( $^3P$ ) + Propene Reaction from Multiplexed Photoionization Mass Spectrometry**

**Supporting Information**

John D. Savee, Oliver Welz, Craig A. Taatjes, and David L. Osborn<sup>\*</sup>

Combustion Research Facility, Mail Stop 9055, Sandia National Laboratories, Livermore, CA  
94551-0969 USA

1. Methods for determination of product branching
2. Relative yields and isomeric composition of secondary products
  - 2.1  $m/z = 44$  – Ethenol and acetaldehyde
  - 2.2  $m/z = 28$  – Ethene
  - 2.3  $m/z = 58$  – Stabilized C<sub>3</sub>H<sub>6</sub>O isomers
3. Absolute photoionization cross-section of methyl from threshold to 11 eV

---

<sup>\*</sup> Corresponding Author; email dlosbor@sandia.gov

## 1. Methods for determination of product branching

A time- and energy-dependent signal intensity at a single  $m/z$ ,  $S_{m/z}(t,E)$ , can be obtained by integrating raw  $I(m/z,t,E)$  data over an appropriate  $m/z$  range. Further integrating  $S_{m/z}(t,E)$  over a time window  $\Delta t$  yields the composite photoionization spectrum  $S_{m/z,\Delta t}(E)$ , from which we can determine whether more than one isomer contributes to the observed signal at this  $m/z$  ratio over any particular time window  $\Delta t$ . In the absence of multiple isomers at a given  $m/z$ , Eq. 1 relates the signal for species  $i$ ,  $S_i(t,E)$ , to the time-dependent concentration profile of species  $i$ ,  $N_i(t)$ .

$$S_i(t, E) = \Lambda \cdot \alpha(m/z) \cdot N_i(t) \cdot \sigma_i(E) \quad (1)$$

Here  $\sigma_i(E)$  is the energy-dependent absolute photoionization cross-section,  $\alpha(m/z)$  is an instrumental mass discrimination factor, and  $\Lambda$  is a collection of mass-independent instrumental parameters.<sup>1,2</sup> At 298 K and 4 Torr the mass discrimination factor for our photoionization mass spectrometer is well-approximated by the expression  $\alpha(m/z) = (m/z)^{0.643}$ .<sup>3</sup> To extract the highest signal-to-noise time profiles, we integrate  $S_i(t,E)$  over an appropriate energy range  $\Delta E$ ,  $(S_{i,\Delta E}(t) = \int S_i(t, E) dE)$ , and use this quantity (which will henceforth be denoted simply  $S_i(t)$ ) in the kinetic fits discussed below. This time trace,  $S_i(t)$ , can be related to the time-dependent concentration profile  $N_i(t)$  when normalized by the integrated photoionization cross section in the energy range  $\Delta E$ :

$$N_i(t) = \frac{1}{\Lambda \cdot \alpha(m/z)} \frac{S_i(t)}{\int \sigma_i(E) dE} \quad (2)$$

The photoionization energy integration range,  $\Delta E$ , will be explicitly stated in the following discussions. Note that we eliminate the instrument parameter  $\Lambda$  when we evaluate branching ratios  $N_i(t) / N_j(t)$ .

Both stable and transient species are observed in the present experiments, and in order to quantify branching to these product channels we employ simple kinetic modeling of measured  $S_i(t)$  data to extract signal that is proportional to the precursor consumption attributed to each product channel. Here, we invoke a pseudo first-order kinetic model of parallel sequential reactions in which  $k'_1 = k_1[\text{C}_3\text{H}_6]$  and  $k'_0 = k_0[\text{NO}_2] + k_{\text{wall}}$



where  $R = \text{O}({}^3\text{P})$ . In Eq. 3,  $S_a$ ,  $S_b$ , etc. are primary products from the  $\text{O}({}^3\text{P}) + \text{C}_3\text{H}_6$  reaction, and  $A$ ,  $B$ , etc., represent secondary products. The total pseudo first-order rate coefficient for depletion of  $\text{O}({}^3\text{P})$  by  $\text{C}_3\text{H}_6$  is  $k'_1 = k'_{1a} + k'_{1b} + k'_{1c} + \dots$ , with the branching fraction for the example of channel 1a given by  $k'_{1a} / k'_1$ .  $k_0$  is the rate coefficient for  $\text{O}({}^3\text{P}) + \text{NO}_2$ , and  $k_{\text{wall}}$  represents all other losses of  $\text{O}({}^3\text{P})$ .

For each sequential reaction, the time-dependence of  $S_i$  can be represented by the integrated rate law for a first-order sequential reaction (Eq. 4) convolved with an appropriate instrument response function.<sup>4-6</sup>

$$S_i(t) = \left( \frac{S'_i \cdot c_{1,i}}{c_{2,i} - c_{1,i}} \right) \cdot \left( e^{-c_{1,i} \cdot t} - e^{-c_{2,i} \cdot t} \right) \tag{4}$$

Here the fit parameter  $S'_i$  is proportional to the amount of reactant consumed to yield primary products  $S_i$ , and  $c_{1,i}$  and  $c_{2,i}$  are the (pseudo-) first order rate constants for formation and loss of product  $S_i$ . In light of the parallel sequential reaction outlined in Eq. 3,  $S'_i$  is equivalent to the fraction of  $R$  consumed to yield  $S_i$ ,  $[R] \cdot k'_{1,i} / k'_1$ , and  $c_{1,i}$  and  $c_{2,i}$  are equivalent to  $k'_1$  and  $k'_{2,i}$ , respectively. When fitting the time profile of a stable product, we set the loss rate  $c_{2,i} = 0$ . Note that this method yields straight-forward interpretation of  $c_{1,i}$  and  $c_{2,i}$  as formation and decay constants in the case where  $c_{1,i} > c_{2,i}$ , which will be true in the present experiments if reaction with  $\text{NO}_2$  is the principal loss mechanism for all transient products generated in R1. Substitution of the fitted  $S'_i$  parameter in place of  $S_i(t)$  in Eq. 2 yields  $N'_i$ , the concentration of precursor consumed for a particular product channel, in place of  $N_i(t)$ . Branching ratios are reported relative to the methyl radical (i.e.,  $N'_i / N'_{\text{methyl}}$ ) representing channel R1c.

For transient species where  $c_{2,i} \neq 0$ , a high degree of correlation was observed between the fitted  $c_{1,i}$  and  $c_{2,i}$  parameters. This correlation is apparent from an almost negligible (< 6%) change in  $\chi^2$  values for fits where  $c_{1,i}$  was fixed at values from  $1200 - 2500 \text{ s}^{-1}$ . This behavior implies that we are not very sensitive to the value of  $c_{1,i}$  in the fits to transient species. However, the  $S'_i$  values determined by fixing  $c_{1,i}$  over the previously mentioned range of values did not affect the measured branching ratios significantly outside of the reported uncertainties and we conclude that the methods used here deliver robust determinations of product branching.

The results from this fit of the kinetic traces to Eq. 4 (unscaled for additional contributions outlined in the main text) are presented in Table S1. Unfortunately, the mass resolution of the mass spectrometer can fluctuate from day-to-day, and while most of the data presented in Table S1 is from one photoionization scan, the high mass resolution required to

resolve ethyl signal from  $m/z = 29$  was achieved in a separate but lower signal-to-noise scan. Ethyl radical signal was compared to methyl signal in this data set using the values enclosed by parentheses in Table S1.

## 2. Relative yields and isomeric composition of secondary products

As discussed in the main text, the observed kinetics for the products at  $m/z = 28$ , 44, and 58 suggest that they are largely formed via secondary chemistry. Nevertheless, the isomeric composition of these species and their branching ratios relative to methyl from the title reaction can be determined as described below.

### 2.1 $m/z = 44$ – Ethenol and acetaldehyde

The time profile obtained from integrating the  $m/z = 44$  product signal from  $O(^3P) + C_3H_6$  between 8.215 and 10.990 eV is suggestive of a stable product (Fig. S1(a)), and the location of the peak in the mass spectrum obtained by further integration from 0 to 50 ms after photolysis indicates a sum formula of  $C_2H_4O$  ( $m/z = 44.026$ ). A fit of the time profile for  $m/z = 44$  to Eq. 4 is shown in Fig. S1(a) and Table S1. The photoionization spectrum for  $m/z = 44$  between 0 and 50 ms after photolysis is shown in Fig S1(b) and appears to have an onset near 9.3 eV and a sharp inflection point near 10.2 eV. The observed  $m/z = 44$  photoionization spectrum is reasonably well-described by contributions from ethenol<sup>7</sup> ( $CH_2CHOH$ , AIE = 9.33 eV)<sup>8</sup> and acetaldehyde<sup>9</sup> ( $CH_3CHO$ , AIE = 10.22 eV)<sup>10</sup> with respective branching fractions ( $\chi_i$ ) of 0.16 and 0.84 (red trace in Fig. S1(b)). Time traces from integration between 8.215 and 10.215 eV (which should include only ethenol) were found to be equivalent within signal-to-noise to those obtained between 10.215 and 10.990 eV (ethenol + acetaldehyde).

Integration of the absolute photoionization cross-sections for ethenol and acetaldehyde from 8.215 to 10.990 eV yields values of  $(11.44 \pm 2.29)$  Mb eV for ethenol and  $(6.47 \pm 1.29)$  Mb eV for acetaldehyde. The total effective photoionization cross-section,  $\sum_i (\chi_i \cdot \int \sigma_i(E) \cdot dE)$ , along with the mass discrimination factor can be used with the fit to the  $m/z = 44$  time trace to evaluate the total  $m/z = 44$  branching ratio of  $(0.50 \pm 0.15)$  relative to methyl or individual branching ratios of  $(0.42 \pm 0.13)$  and  $(0.08 \pm 0.02)$  for acetaldehyde and ethenol, respectively.

## 2.2 $m/z = 28$ – Ethene

The time trace for the  $m/z = 28$  product signal obtained by integrating between 8.215 and 10.990 eV is consistent with a stable product and is shown in Fig. S2(a) along with the corresponding fit to Eq. 4 (red trace). The photoionization spectrum obtained for this species from integration between 0 and 50 ms after photolysis is shown in Fig. S2(b), and is clearly due to ethene based on similarity to the measured photoionization cross-section for this species (Table S2). Evaluation of the fit of the data and the integrated photoionization cross-section for ethene yields a branching ratio of  $(0.34 \pm 0.10)$  relative to methyl. For both  $O(^3P) + CH_3CDCH_2$  and  $O(^3P) + CH_3CHCD_2$  evidence for ethene appears at  $m/z = 29$  (note that signal at  $m/z = 30$  may be obscured by signal from NO). Mechanistically, the simplest route to form ethene after terminal addition of  $O(^3P)$  to propene is a H atom shift from C<sub>3</sub> to C<sub>2</sub> followed by cleavage of the C<sub>1</sub>-C<sub>2</sub> bond on the singlet C<sub>3</sub>H<sub>6</sub>O PES. Although observation of  $m/z = 29$  in the case of  $O(^3P) + CH_3CDCH_2$  is consistent with this simple mechanism, the observation of ethene at  $m/z = 29$  from  $O(^3P) + CH_3CHCD_2$  indicates that either a more complex mechanism exists for production of ethene (which are certainly suggested based on minimum energy paths outlined in the main text) or that at least some of the ethene produced is the result of secondary chemistry. Based on other

evidence outlined in the text, we conclude that the latter is the dominant source of ethene observed here.

The anticipated co-product of ethene from the O(<sup>3</sup>P) + propene reaction is formaldehyde (H<sub>2</sub>CO) at *m/z* = 30. Fig. S2(c) presents the photoionization spectrum for *m/z* = 30 from O(<sup>3</sup>P) + propene integrated from 0 to 50 ms after photolysis. The spectrum is clearly dominated by signal from NO (from direct photolysis of NO<sub>2</sub> or secondary chemistry),<sup>11</sup> although a sharp rise is observed near the AIE of formaldehyde at 10.88 eV.<sup>12</sup> An absolute photoionization cross-section for formaldehyde is available in the literature,<sup>13</sup> however the coarseness of the available spectrum coupled with the small energy range and sharp rise of the formaldehyde signal in the present experiments does not allow for quantification of relative concentrations. Formaldehyde signal is observed at *m/z* = 30 and 31 in reactions of O(<sup>3</sup>P) with both deuterated precursors, which, like the signal observed for ethene isotopomers, indicates that either the mechanism for producing ethene + formaldehyde is complex or that formaldehyde is a product from unknown secondary chemistry.

### 2.3 *m/z* = 58 – Stabilized C<sub>3</sub>H<sub>6</sub>O isomers

Product signal at *m/z* = 58, the mass corresponding to the stabilization product of the O(<sup>3</sup>P) + C<sub>3</sub>H<sub>6</sub> reaction, was also observed. The time trace obtained from data integrated between 8.215 and 10.990 eV indeed indicates formation of a stable product. Integration of the data between 8.215 and 10.990 eV and 0 to 50 ms after photolysis yields a mass spectrum that is consistent with a sum formula of C<sub>3</sub>H<sub>6</sub>O (*m/z* = 58.042) for this product. A fit of the time trace is shown in red in Fig. S3(a), and the fit parameters are included in Table S1. As discussed in the main text, the slow rise relative to e.g., methylketene (see Fig. 4 of the main text) and the

inflection point in the rising feature are strong indications that C<sub>3</sub>H<sub>6</sub>O is not formed directly from the O(<sup>3</sup>P) + C<sub>3</sub>H<sub>6</sub> reaction, but rather from secondary chemistry.

The photoionization spectrum for *m/z* = 58 for kinetic times between 0 and 50 ms after photolysis is shown by the black circles in Fig. S3(b). Several C<sub>3</sub>H<sub>6</sub>O isomers have been identified as significant products in past investigation of O(<sup>3</sup>P) + C<sub>3</sub>H<sub>6</sub> near atmospheric pressure, with major products being methyloxirane (CH<sub>3</sub>CH(O)CH<sub>2</sub>) and propanal (CH<sub>3</sub>CH<sub>2</sub>CHO).<sup>14</sup> Acetone (CH<sub>3</sub>COCH<sub>3</sub>) is also a potential product, although at atmospheric pressure<sup>14</sup> it is not formed in significant quantities (reported < 10% of the propanal concentration). At lower pressures the significance of this stabilization channel should decrease as bimolecular channels become more significant, although previous photoionization mass spectrometry experiments under collisionless conditions have still been able to identify a minor C<sub>3</sub>H<sub>6</sub>O product.<sup>15</sup> However, as outlined in the main text, some evidence exists for secondary product formation in those experiments. The absence of C<sub>3</sub>H<sub>6</sub>O signal in the collisionless and low-pressure (< 7.5 Torr) experiments of Blumentberg *et al.*<sup>16</sup> agrees with our conclusion that no significant amount of C<sub>3</sub>H<sub>6</sub>O is produced as a primary product in our experiments at 4 torr and 298 K.

Absolute photoionization spectra for the three C<sub>3</sub>H<sub>6</sub>O isomers considered previously (acetone,<sup>9</sup> propanal,<sup>17</sup> and methyloxirane (Table S3) are shown in Fig. S3(c). Of these three isomers, acetone has the lowest AIE (9.70 eV).<sup>18</sup> The onset of signal in the *m/z* = 58 photoionization spectrum is at ~ 8.7 eV, well below the AIE of acetone and it is clear that, in the absence of *m/z* = 58 signal from dissociative ionization of a higher mass species, another C<sub>3</sub>H<sub>6</sub>O species contributes to the observed signal. The onset of the *m/z* = 58 photoionization spectrum is consistent with this product being one or a combination of the propenols, the most

mechanistically plausible being the *E* or *Z* isomers of 1-propen-1-ol ( $\text{CH}_3\text{CHCHOH}$ ,  $\text{AIE}_E = 8.64$  eV and  $\text{AIE}_Z = 8.70$  eV)<sup>19</sup> or 1-propen-2-ol ( $\text{CH}_3\text{COHCH}_2$ ,  $\text{AIE} = 8.6 - 8.7$  eV).<sup>20,21</sup> A photoionization spectrum for *Z*-1-propen-1-ol has been previously simulated from Franck-Condon factors using Gaussian09<sup>22</sup> and the CBS-QB3 method for calculation of geometries, force constants, and harmonic frequencies of the neutral and cation ground electronic states.<sup>17</sup> The resulting spectrum was scaled to a value of 17 Mb above the Franck-Condon envelope based, in part, on simple bond-additivity models for estimating photoionization cross-sections<sup>23</sup> and is included as the yellow trace in Fig. S3(c). Although we cannot rule out contributions from other propenol isomers (e.g., *E*-1-propen-1-ol, 1-propen-2-ol), the *Z*-1-propen-1-ol spectrum is used to estimate the total contribution from propenol isomers in the  $m/z = 58$  photoionization spectrum.

A fit to the  $m/z = 58$  spectrum using the absolute photoionization cross-sections presented in Fig. S3(c) yields the  $m/z = 58$  branching fractions  $\chi_{\text{methyloxirane}} = 0.71$ ,  $\chi_{\text{propanal}} = 0.14$ ,  $\chi_{\text{acetone}} = 0.10$ , and  $\chi_{\text{propenols}} = 0.05$ . The fit to  $m/z = 58$  using these branching fractions is shown by the red trace in Fig. S3(b). The derived value for acetone depends heavily on the shape of the *Z*-1-propen-1-ol photoionization spectrum between 9.7 and 10 eV (near the AIE of propanal) and may be overestimated using the simulated propenol spectrum. No significant difference is apparent in the time traces obtained between 8.215 and 9.815 eV (only propenols) and those obtained between 10.215 and 10.990 eV (all  $m/z = 58$  isomers). Using these branching fractions determined for the  $\text{C}_3\text{H}_6\text{O}$  isomers allows the measured  $m/z = 58$  signal to be weighted and compared to the methyl radical yield in R1, resulting in branching ratios of  $(0.28 \pm 0.07)$ ,  $(0.05 \pm 0.01)$ ,  $(0.04 \pm 0.01)$ , and  $(0.02 \pm 0.01)$  for methyloxirane, propanal, acetone, and *Z*-1-propen-1-ol, respectively.

### 3. Absolute photoionization cross-section of methyl from threshold to 11 eV

Photolysis of acetone at 4 Torr and 298 K using 193 nm photons was carried out to generate a relative photoionization spectrum for the methyl radical between 9.5 and 11.0 eV. This relative spectrum was placed on an absolute scale using literature values for the photoionization cross-section at single energies.<sup>3,24,25</sup> The resulting values are presented in Table S4.

### References

- (1) T. A. Cool, A. McIlroy, F. Qi, P. R. Westmoreland, L. Poisson, D. S. Peterka, and M. Ahmed. *Rev. Sci. Instrum.*, 2005, **76**, 094102.
- (2) D. L. Osborn, P. Zou, H. Johnsen, C. C. Hayden, C. A. Taatjes, V. D. Knyazev, S. W. North, D. S. Peterka, M. Ahmed, and S. R. Leone. *Rev. Sci. Instrum.*, 2008, **79**, 104103.
- (3) J. D. Savee, S. Soorkia, O. Welz, T. M. Selby, C. A. Taatjes, and D. L. Osborn. *J. Chem. Phys.*, 2012, in press.
- (4) O. Welz, J. D. Savee, D. L. Osborn, S. S. Vasu, C. J. Percival, D. E. Shallcross, and C. A. Taatjes. *Science*, 2012, **335**, 204.
- (5) C. A. Taatjes. *Int. J. Chem. Kinet.*, 2007, **39**, 565.
- (6) S. B. Moore and R. W. Carr. *Int. J. Mass Spectrom. Ion Process.*, 1977, **24**, 161.
- (7) T. A. Cool, K. Nakajima, T. A. Mostefaoui, F. Qi, A. McIlroy, P. R. Westmoreland, M. E. Law, L. Poisson, D. S. Peterka, and M. Ahmed. *J. Chem. Phys.*, 2003, **119**, 8356.
- (8) B. Ruscic and J. Berkowitz. *J. Chem. Phys.*, 1994, **101**, 10936.
- (9) O. Welz, J. Zador, J. D. Savee, M. Y. Ng, G. Meloni, R. X. Fernandes, L. Sheps, B. A. Simmons, T. S. Lee, D. L. Osborn, and C. A. Taatjes. *Phys. Chem. Chem. Phys.*, 2012, **14**, 3112.
- (10) J. C. Traeger. *Int. J. Mass Spectrom. Ion Process.*, 1985, **66**, 271.
- (11) K. Watanabe, Matsunag.Fm, and H. Sakai. *Appl. Optics*, 1967, **6**, 391.
- (12) N. I. S. T. Webbook.
- (13) G. Cooper, J. E. Anderson, and C. E. Brion. *Chem. Phys.*, 1996, **209**, 61.

- (14) R. J. Cvetanovic. *Can. J. Chem.-Rev. Can. Chim.*, 1958, **36**, 623.
- (15) J. R. Kanofsky and D. Gutman. *Chem. Phys. Lett.*, 1972, **15**, 236.
- (16) B. Blumenberg, K. Hoyermann, and R. Sievert. *16th Int. Symp. on Combust. 1976, The Combustion Institute*, 1977, 841.
- (17) O. Welz, J. D. Savee, A. J. Eskola, L. Sheps, D. L. Osborn, and C. A. Taatjes. *Proc. Combust. Inst.*, 2013, **34**, in review.
- (18) J. C. Traeger, R. G. McLoughlin, and A. J. C. Nicholson. *J. Am. Chem. Soc.*, 1982, **104**, 5318.
- (19) F. Turecek. *J. Chem. Soc.-Chem. Commun.*, 1984, 1374.
- (20) M. Iraqi, I. Pribar, and C. Lifshitz. *Org. Mass Spectrom.*, 1986, **21**, 661.
- (21) F. Turecek and V. Hanus. *Org. Mass Spectrom.*, 1984, **19**, 631.
- (22) M. J. Frisch, G. W. Trucks, H. B. Schlegel, G. E. Scuseria, M. A. Robb, J. R. Cheeseman, G. Scalmani, V. Barone, B. Mennucci, G. A. Petersson, H. Nakatsuji, M. Caricato, X. Li, H. P. Hratchian, A. F. Izmaylov, J. Bloino, G. Zheng, J. L. Sonnenberg, M. Hada, M. Ehara, K. Toyota, R. Fukuda, J. Hasegawa, M. Ishida, T. Nakajima, Y. Honda, O. Kitao, H. Nakai, T. Vreven, J. A. Montgomery, J. E. Peralta, F. Ogliaro, M. Bearpark, J. J. Heyd, E. Brothers, K. N. Kudin, V. N. Staroverov, R. Kobayashi, J. Normand, K. Raghavachari, A. Rendell, J. C. Burant, S. S. Iyengar, J. Tomasi, M. Cossi, N. Rega, J. M. Millam, M. Klene, J. E. Knox, J. B. Cross, V. Bakken, C. Adamo, J. Jaramillo, R. Gomperts, R. E. Stratmann, O. Yazyev, A. J. Austin, R. Cammi, C. Pomelli, J. W. Ochterski, R. L. Martin, K. Morokuma, V. G. Zakrzewski, G. A. Voth, P. Salvador, J. J. Dannenberg, S. Dapprich, A. D. Daniels, Farkas, J. B. Foresman, J. V. Ortiz, J. Ciosowski, and D. J. Fox. Gaussian 09, Revision B.01 Wallingford CT, 2009.
- (23) M. Bobeldijk, W. J. Vanderzande, and P. G. Kistemaker. *Chem. Phys.*, 1994, **179**, 125.
- (24) C. A. Taatjes, D. L. Osborn, T. M. Selby, G. Meloni, H. Y. Fan, and S. T. Pratt. *J. Phys. Chem. A*, 2008, **112**, 9336.
- (25) B. Gans, L. A. V. Mendes, S. Boye-Peronne, S. Douin, G. Garcia, H. Soldi-Lose, B. K. C. de Miranda, C. Alcaraz, N. Carrasco, P. Pernot, and D. Gaujacq. *J. Phys. Chem. A*, 2010, **114**, 3237.

Table S1. Parameters from fitting the observed kinetic traces between 8.215 and 10.990 eV (except where noted) to the time-dependence of the intermediate product in a first-order sequential reaction (Eq. 4) for various mass channels produced in the O(<sup>3</sup>P) + C<sub>3</sub>H<sub>6</sub> reaction at 298 K and 4 Torr. Reported errors are 2σ uncertainties from the fitting procedure. Values in parenthesis are from a lower signal-to-noise but higher mass resolution data set used to separate HCO from C<sub>2</sub>H<sub>5</sub> signal.

<b><i>m/z</i></b>	<b>species</b>	<b><i>S'</i> (Arb. Units)</b>	<b><i>c</i><sub>1</sub> (s<sup>-1</sup>)</b>	<b><i>c</i><sub>2</sub> (s<sup>-1</sup>)</b>	<b><math>\int \sigma_i(E) \cdot dE</math> (Mb eV)</b>
15 <sup>a</sup>	methyl	5.73 ± 3.50 (0.46 ± 0.06)	1690 ± 1290	1090 ± 720	1.80 ± 0.36
28	ethene	3.29 ± 0.18	610 ± 220	0	2.53 ± 0.51
29 <sup>b</sup>	formyl, ethyl	(2.17 ± 0.20)	2210 ± 720	1490 ± 420	5.44 ± 1.09
44	acetaldehyde, ethenol	18.8 ± 0.6	533 ± 110	0	7.27 ± 1.50
56	methylketene	17.5 ± 0.3	1140 ± 180	0	44.77 ± 8.95
58	methyloxirane, propanal, acetone, Z-1-propen-1-ol	18.2 ± 0.3	560 ± 70	0	7.42 ± 0.84

<sup>a</sup>Integrated between 8.215 and 10.215 eV

<sup>b</sup>Integrated from 8.215 to 10.015 eV and 29.02 to 29.07 amu.

Table S2. Absolute photoionization cross-section of ethene at 298 K measured relative to propene.<sup>9</sup>

<b>Photoionization Energy (eV)</b>	<b><math>\sigma</math> (Mb) <i>m/z</i> = 28</b>	<b>Photoionization Energy (eV)</b>	<b><math>\sigma</math> (Mb) <i>m/z</i> = 28</b>
10.003	0.00	10.528	1.77
10.028	0.00	10.553	2.56
10.053	0.00	10.578	3.08
10.078	0.00	10.603	3.21
10.103	0.00	10.628	3.49
10.128	0.00	10.653	3.40
10.153	0.00	10.678	4.27
10.178	0.01	10.703	5.09
10.203	0.01	10.728	5.46
10.228	0.01	10.753	5.82
10.253	0.00	10.778	5.97
10.278	0.00	10.803	6.19
10.303	0.01	10.828	6.66
10.328	0.00	10.853	6.79
10.353	0.01	10.878	6.63
10.378	0.03	10.903	7.23
10.403	0.01	10.928	7.15
10.428	0.05	10.953	7.95
10.453	0.05	10.978	7.09
10.478	0.16	11.003	7.70
10.503	1.03		

Table S3. Absolute photoionization cross-section of methyloxirane at 298 K measured relative to propene.

<b>Photoionization Energy (eV)</b>	<b><math>\sigma</math> (Mb) <math>m/z = 58</math></b>	<b><math>\sigma</math> (Mb) <math>m/z = 57</math></b>	<b><math>\sigma</math> (Mb) <math>m/z = 45</math></b>	<b><math>\sigma</math> (Mb) <math>m/z = 43</math></b>	<b><math>\sigma</math> (Mb) <math>m/z = 30</math></b>
9.813	0.00	0.00	0.00	0.00	0.00
9.838	0.00	0.00	0.00	0.00	0.00
9.863	0.00	0.00	0.00	0.00	0.00
9.888	0.01	0.00	0.00	0.00	0.00
9.913	0.01	0.00	0.00	0.00	0.00
9.938	0.01	0.00	0.00	0.00	0.00
9.963	0.01	0.01	0.00	0.00	0.00
9.988	0.02	0.00	0.00	0.00	0.00
10.013	0.03	0.00	0.00	0.00	0.00
10.038	0.06	0.01	0.00	0.00	0.00
10.063	0.13	0.00	0.00	0.00	0.00
10.088	0.11	0.01	0.00	0.00	0.00
10.113	0.16	0.00	0.00	0.00	0.00
10.138	0.26	0.00	0.00	0.00	0.00
10.163	0.45	0.01	0.00	0.00	0.00
10.188	0.66	0.00	0.00	0.00	0.00
10.213	1.02	0.01	0.00	0.01	0.00
10.238	1.90	0.00	0.00	0.00	0.00
10.263	2.38	0.01	0.00	0.00	0.00
10.288	2.68	0.00	0.00	0.01	0.00
10.313	3.33	0.01	0.00	0.00	0.00
10.338	3.59	0.00	0.00	0.01	0.00
10.363	3.86	0.01	0.00	0.00	0.00
10.388	4.72	0.01	0.00	0.01	0.00
10.413	5.17	0.01	0.00	0.01	0.00
10.438	5.37	0.00	0.00	0.00	0.00
10.463	5.71	0.01	0.00	0.01	0.00
10.488	5.94	0.00	0.00	0.01	0.00
10.513	6.50	0.00	0.00	0.02	0.00
10.538	6.66	0.01	0.00	0.03	0.00
10.563	6.93	0.01	0.00	0.02	0.00
10.588	7.03	0.01	0.00	0.01	0.00
10.613	7.09	0.01	0.00	0.04	0.00
10.638	7.55	0.02	0.02	0.02	0.01
10.663	7.53	0.02	0.02	0.06	0.00
10.688	7.82	0.02	0.02	0.07	0.01
10.713	8.02	0.03	0.03	0.06	0.02
10.738	8.06	0.04	0.01	0.09	0.02
10.763	8.21	0.04	0.03	0.16	0.05
10.788	8.19	0.05	0.03	0.17	0.01

10.813	8.10	0.06	0.03	0.22	0.05
10.838	8.06	0.07	0.04	0.34	0.07
10.863	8.20	0.12	0.04	0.40	0.06
10.888	8.11	0.17	0.05	0.42	0.06
10.913	8.04	0.15	0.04	0.57	0.11
10.938	7.95	0.26	0.04	0.58	0.17
10.963	7.83	0.31	0.05	0.60	0.21
10.988	8.06	0.27	0.02	0.84	0.18

Table S4. Absolute photoionization cross-section of the methyl radical at 298 K

<b>Photionization Energy (eV)</b>	<b><math>\sigma</math> (Mb) <math>m/z = 15</math></b>	<b>Photionization Energy (eV)</b>	<b><math>\sigma</math> (Mb) <math>m/z = 15</math></b>
9.500	0.00	10.275	5.75
9.525	0.00	10.300	5.80
9.550	0.00	10.325	5.68
9.575	0.00	10.350	5.63
9.600	0.00	10.375	5.72
9.625	0.00	10.400	5.80
9.650	0.00	10.425	5.42
9.675	0.01	10.450	5.85
9.700	0.02	10.475	5.86
9.725	0.03	10.500	5.52
9.750	0.09	10.525	5.30
9.775	0.15	10.550	5.81
9.800	0.31	10.575	6.08
9.825	1.82	10.600	5.73
9.850	3.68	10.625	5.70
9.875	4.28	10.650	5.89
9.900	4.26	10.675	5.66
9.925	4.18	10.700	5.73
9.950	4.19	10.725	5.76
9.975	4.39	10.750	5.77
10.000	4.54	10.775	5.99
10.025	4.87	10.800	5.78
10.05	4.54	10.825	5.88
10.075	4.80	10.850	5.52
10.100	4.81	10.875	5.60
10.125	4.64	10.900	5.57
10.150	5.29	10.925	5.69
10.175	5.14	10.950	5.69
10.200	5.29	10.975	5.46
10.225	5.34	11.000	5.15
10.250	5.34		

## Figures

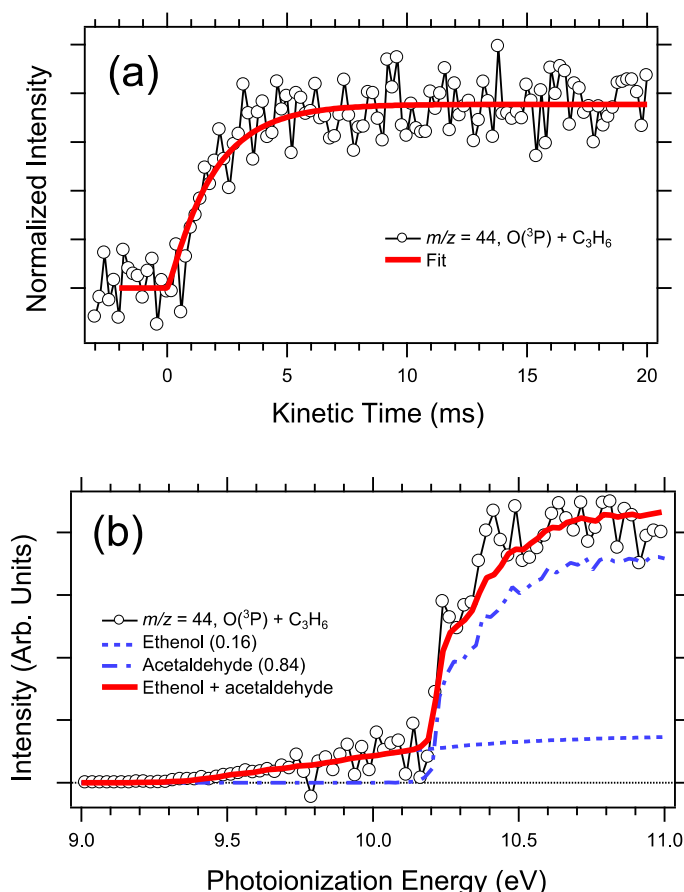


Figure S1. (a) Time trace obtained for the  $m/z = 44$  products from  $O(^3P)$  + propene obtained by integration between 8.215 and 10.990 eV. The red trace is a fit of the data as described here, the results of which are presented in Table S1. (b) Photoionization spectrum for  $m/z = 44$  between 0 and 50 ms after photolysis. The red trace is a fit of the data to known absolute photoionization spectra for ethenol (scaled by 0.16) and acetaldehyde (scaled by 0.84).

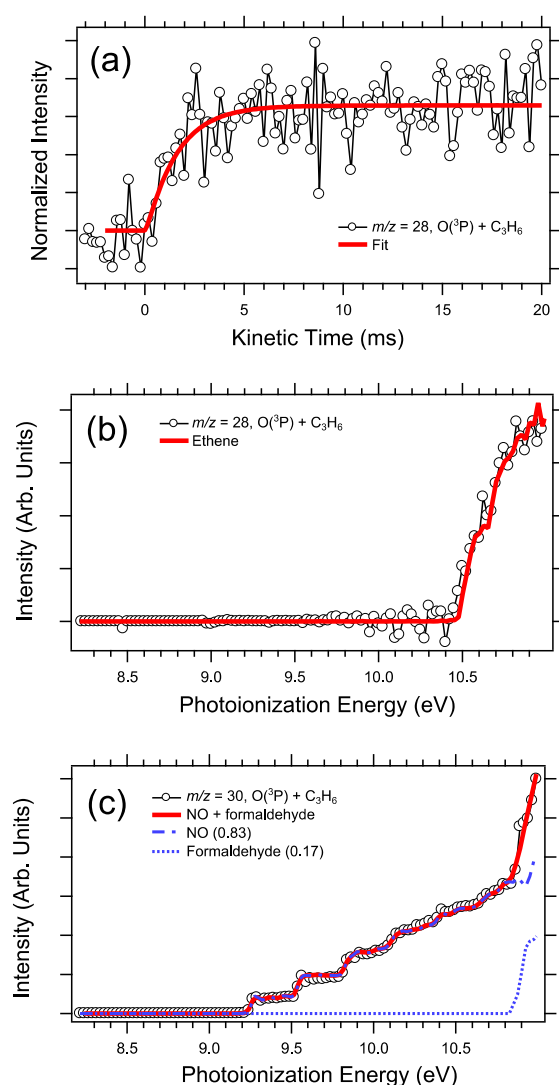


Figure S2. (a) Time trace for the  $m/z = 28$  product from  $O(^3P) + C_3H_6$  obtained by integration between 8.215 and 10.990 eV along with a fit (red trace). (b) Photoionization spectrum for  $m/z = 28$  from 0 to 50 ms after photolysis (black circles) and the photoionization spectrum for ethene (red trace). (c) Photoionization spectrum for  $m/z = 30$  from  $O(^3P) + C_3H_6$  from 0 to 50 ms after photolysis (black circles) and a fit to a linear combination of the photoionization spectra for NO and formaldehyde (red trace).

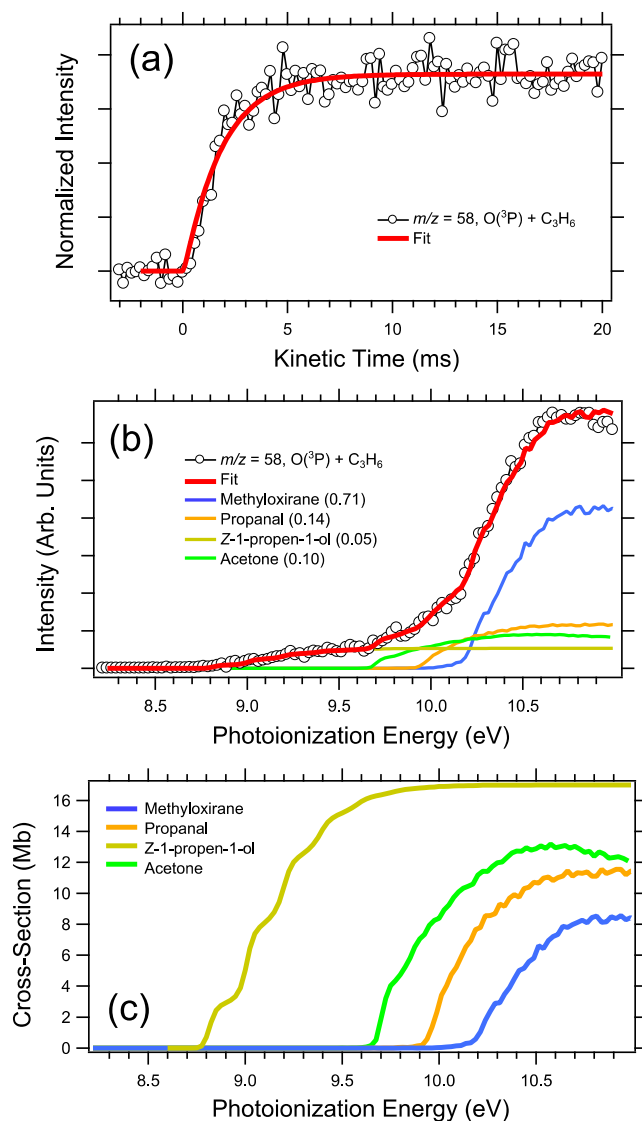


Figure S3. (a) Time trace obtained via integration of the  $m/z = 58$  product signal from the  $\text{O}({}^3\text{P}) + \text{C}_3\text{H}_6$  reaction between 8.215 and 10.990 eV (black circles). The red trace is a fit to the data using the methods outlined in the text. (b) Photoionization spectrum for  $m/z = 58$  obtained by integrating  $\text{O}({}^3\text{P}) + \text{C}_3\text{H}_6$  data between 0 and 50 ms after photolysis. The red trace in (b) is a fit obtained by scaling contributions from the absolute photoionization spectra for different C<sub>3</sub>H<sub>6</sub>O isomers shown in frame (c).